Nonlinear Charge Spreading Visualized in Voltage-Controlled Lateral Superlattices

J. Krauß,[1] A. Wixforth,[1] A. V. Kalameitsev,[2] A. O. Govorov,[2,3] W. Wegscheider,[4] and J. P. Kotthaus[1]

[1]*Sektion Physik and CeNS, Ludwig-Maximilians-Universität München, Geschwister-Scholl-Platz 1, D-80539 München, Germany*
[2]*Institute of Semiconductor Physics, Russian Academy of Sciences—Sibirian Branch,*
Lavrent'eva Avenue 13, Novosibirsk 630090 Russia
[3]*Department of Physics & Astronomy, Ohio University, Clippinger Labs, Athens, Ohio 45701-2979*
[4]*Institut für Angewandte und Experimentelle Physik, Universität Regensburg, D-93040 Regensburg, Germany*

Voltage-controlled lateral potential superlattices are used to dramatically increase the lifetime of photo-generated carriers in a quantum well. These long lifetimes, together with the ability to deliberately trigger radiative recombination, enable us to directly visualize the spreading character of nonlinear Maxwell relaxation of 2D charges along narrow channels. Our system allows for temporal and spatial resolution of Maxwell kinetics, usually a very fast process and difficult to observe. The observed spreading dynamics of a 2D hole plasma is in perfect agreement with our nonlinear model.

The dynamics of charge carriers in solids and plasmas is of fundamental interest as it governs most any optical and electrical response to external perturbations. The decay of nonequilibrium charge in space and time originates from electrostatic repulsion and is described by the Maxwell relaxation [1] which is very fast in most systems and depends on dimensionality. For instance, nonequilibrium bulk charges in a conductive solid decay without any spreading. It was theoretically shown that in the linear 2D regime, however, this relaxation is qualitatively different from the 3D case and has a character of spreading [2–4]. We are able to directly measure this 2D relaxation of charge in a strongly nonlinear regime, where it is considerably slower than in the linear case.

Experimentally, the evolution of nonequilibrium carriers was examined e.g., in bulk systems in the regime of ambipolar diffusion by Haynes and Shockley [5] and in 2D in n-i-p-i doping superlattices [6,7], there referred to as "giant ambipolar diffusion coefficient." However, in all these experiments, carrier dynamics is ambipolar, electrons and holes are strongly coupled, and carrier motion is restricted to the doped regions of the sample.

Here, we would like to demonstrate carrier motion and charge spreading in a unipolar system in the absence of doping. In our experiments, the carriers are confined to an undoped quantum well (QW), and electrons and holes move independently as they are screened from each other by metallic gates. This can be achieved by the use of voltage-controlled lateral superlattices. Such systems offer efficient potential modulation in the plane of the QW. In addition, the amplitude can be tuned and may be modulated with time. This flexibility makes them a useful tool to study a variety of physical phenomena such as the two-dimensional Franz-Keldysh effect [8], collective excitations [9], and the trapping of excitons [10]. In particular, a small-scale lateral type-II potential modulation can be obtained to ionize photogenerated excitons and to laterally separate the carriers. This leads, as in analogous structures [11,12], to a dramatic increase of the carrier lifetimes. Moreover, in voltage-controlled structures, an almost arbitrary lifetime is combined with the unique possibility to spontaneously initiate fast radiative recombination [13,14]. A photonic-memory device based on this concept has been recently introduced [13].

The sample employed was grown by molecular beam epitaxy on a (001)-oriented semi-insulating GaAs substrate. It consists of an undoped GaAs-AlAs buffer, a 4×10^{18} cm^{-3} Si-doped backcontact, 300 nm $Al_{03}Ga_{0.7}As$ rear barrier, an undoped 20 nm wide GaAs QW, 40 nm $Al_{0.5}Ga_{0.5}As$ top barrier, and 5 nm GaAs cap. The barriers are short-period superlattices to avoid vertical leakage currents.

To achieve the lateral modulation, two highly conductive aluminum electrodes are evaporated on top of the sample, forming an interdigitated structure of 400×500 μm^2. Electrode-finger width w and spacing s are 1 μm. Each electrode is flanked by a large bond pad. Applying different voltages V_1 and V_2 between the electrodes and the backcontact results in a stripelike lateral potential modulation in the QW layer according to the voltage difference $\Delta V = V_1 - V_2$.

To study space- and time-resolved photoluminescence (PL) at low temperatures, the sample is mounted in an optical cryostat. We employ a setup similar to a fluorescence microscope with a pulsed laser diode (680 nm) as the excitation source, a RG780 color filter, and a fast, gated intensified CCD camera. Thus, we can record entire images of the luminescent light of the sample with a temporal resolution of 0.3 ns and a spatial resolution of about 2 μm. Up to 1000 frames at a repetition rate of 20 kHz are accumulated to generate an image. To visualize two-dimensional carrier dynamics, we perform a modified storage experiment in analogy to the photonic memory device [13]: The possibility to deliberately trigger radiative recombination

at any given moment after the optical excitation enables us to take "snapshots" of the actual carrier distribution in the sample in a stroboscopic manner.

A sketch of the setup (not to scale) is given in Fig. 1(a): The laser is focused to a line in the center of the interdigitated structure. The width (FWHM) of the spot is about 10 μm, the length covers about 180 μm or 45 fingerpairs of the interdigitated electrodes. The voltages V_1 and V_2 are applied at time $t = 0$ ns, when the sample is illuminated by a 15 ns laser pulse. Photogenerated excitons are ionized and electrons/holes are stored underneath the positive/negative electrode, respectively. After a certain storage time $t = t_s$ the bias is removed. The carriers are no longer confined beneath the electrodes and recombine radiatively within about 15 ns. This actually limits the temporal resolution of the experiment.

As long as the bias is applied, the carriers are confined to stripes in the voltage-induced potential wells. Carrier motion is essentially possible only in one dimension along these stripes (x direction). Free motion in the perpendicular direction (y direction) is possible only after removing the bias, leading to radiative recombination and therefore annihilation of the carriers on a time scale being fast compared to the carrier motion along x. Thus, the luminescence pattern along the x direction directly corresponds

to the carrier distribution at time $t = t_s$. The PL images recorded by the camera are, to some extent, snapshots of the carrier profile at t_s.

Such pictures [15] taken at a carrier density of about 3×10^{11} cm^2 and $T = 4$ K are plotted in part (b) of Fig. 1 (cf. scaling below). The three pictures are recorded on a logarithmic intensity scale at times $t_s = 10$, 60, and 260 ns after the laser pulse, respectively. One can clearly recognize the evolution of the PL pattern with time.

Several characteristics have to be pointed out: The luminescent area spreads only in the x direction, i.e., along the electrodes. In the y direction, the original width of the pattern remains essentially constant, in accordance with the explanation above. Furthermore, the image at $t_s = 260$ ns exhibits a clipping of the bright area at about ± 200 μm. This marks the positions of the opaque pads, masking any luminescence arising from the sample.

Also, all images show a bright line in the center, corresponding to the position of the initial laser spot. This inherent "memory" has a time constant of about 1 min. It obviously does not show any dynamic behavior during the experiment. Its origin is not yet fully understood, but may be attributed to locally trapped carriers.

In Part (a) of Fig. 2, central cross sections along the x direction of the corresponding pictures from Fig. 1 are plotted for several times t_s on a linear scale. Again, the
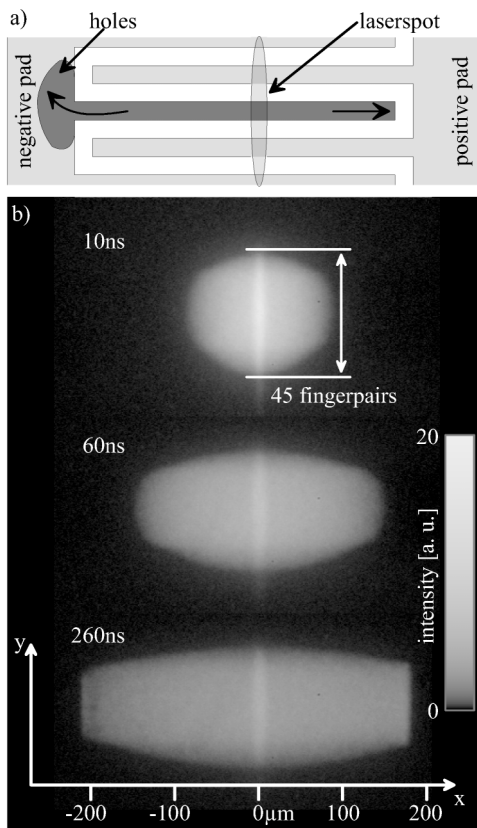

FIG. 1. Sketch of the sample not to scale (a) and snapshots of the luminescence pattern at time $t_s = 10$, 60, and 260 ns after the laser pulse (b), basically representing the actual hole distribution [15].
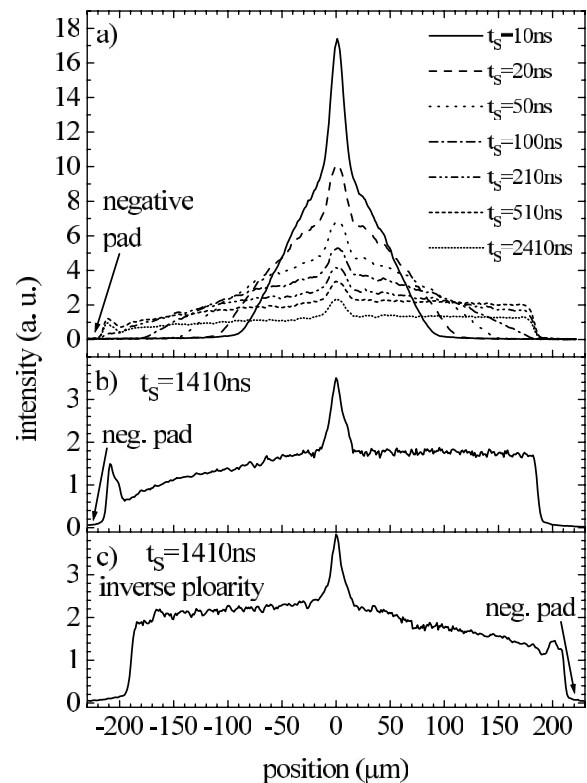

FIG. 2. Cross sections of the luminescence intensity along the x direction at different times t_s (a). Parts (b) and (c) show two measurements with opposite bias (same parameters as in Fig. 1). The peak close to the negative pad is attributed to the field enhancement at the ends of the finger gates.

temporal evolution of the initially narrow distribution and the bright spot in the center are clearly visible. The spatial distribution of intensity is symmetric, unless the diffusing carriers reach the edge of the interdigitated structure. In the plots for $t_s > 200$ ns, the intensity decreases stronger towards negative x values. This fact indicates that the two boundaries defined by the pads cannot be treated equally, as emphasized in the lower parts of Fig. 2: Part (b) shows a plot with the same parameters as discussed previously. For the plot in part (c), the polarity of the voltages has been exchanged. The asymmetric shape is reversed with regard to the position of the laser spot. This indicates that these differences in the boundary conditions are not an artifact, but must be attributed to the voltage-induced potential.

In the following, we will concentrate on the quantitative modeling of the experimental results. Carrier motion is confined to the x direction parallel to the electrodes unless the bias is removed. This already became obvious from Figs. 1 and 2. With the electrode stripe length being much larger than its width w of 1 μm, the electron and hole sheet densities n and p, respectively, can be regarded as constant in the y direction within the time resolution of our experiment. This allows us to use a one-dimensional model to describe 2D carrier motion as currents along the x direction. For simplicity, in the following, all equations are written for holes, e denoting the positive elementary charge.

The motion is driven both by diffusion and drift:

$$j_p = j_{\text{diff}} + \sigma E = -eD_p \frac{\partial p}{\partial x} + ep\mu_p E_x. \quad (1)$$

The latter arises from the electric field E_x originating from the inhomogeneous carrier distribution along x. However, this field is strongly screened by the metal of the interdigitated electrodes, as their distance d to the 2D system (i.e., the quantum-well top barrier) is much smaller than the typical width of the carrier distribution in the x direction L and also much smaller than the electrode width w. Thus the system is similar to a flat capacitor, and the in-plane field in x direction can be approximated as [16]

$$E_x = -\frac{de}{\epsilon_0 \epsilon_r} \frac{\partial p}{\partial x} \qquad (d \ll w, L). \quad (2)$$

On the other hand, the electric fields arising from holes beneath one electrode do not influence electrons beneath the adjacent electrodes and vice versa, as d is short compared to the electrode spacing: $d \gg w$. This essentially decouples the motion of electrons and holes in our system: We have to deal with independent, unipolar carrier motion, in contrast to ambipolar diffusion in n-i-p-i- structures [7]. This fact instantaneously implies two different time scales, as in GaAs the mobility of electrons exceeds the one of holes by about 1 order of magnitude: On the time scale of hole motion, the electron distribution can be regarded as already relaxed and thus to be constant. The luminescence intensity, however, is proportional to the product $n(x) \times p(x)$ of the local electron and the hole density, and its behavior will therefore largely be

governed by the slower carrier type, i.e., the holes. The luminescence pattern thus corresponds almost directly to the local hole density $p(x)$.

In particular, this fact also accounts for the asymmetric voltage-dependent boundaries pointed out earlier: As sketched in part (a) of Fig. 1, the negative pad allows holes to diffuse beneath it. As it is much larger than the interdigitated area, it can be regarded as an ideal sink for holes. Towards the positive pad, the negatively charged electrode stripe ends open, representing a hard wall. In this picture, the asymmetric shape of the carrier distributions in parts (b) and (c) of Fig. 2 and its voltage dependence can be easily understood. Towards the sink, the density must be reduced as compared to the hard wall side.

To obtain a complete quantitative description of hole dynamics in the structure, the conservation of charge can be combined with Eqs. (1) and (2), yielding

$$e \frac{\partial p}{\partial t} = \frac{e^2 d\mu_p}{\epsilon_0 \epsilon_r} \frac{\partial}{\partial x}\left(p \frac{\partial p}{\partial x}\right) + e \frac{\partial}{\partial x}\left(D_p \frac{\partial p}{\partial x}\right). \quad (3)$$

The solution of Eq. (3) is sketched in Fig. 3(c), where we plot the hole density versus position for two different times. For comparison, we also show the solutions of the corresponding linear problem in 3D [Fig. 3(a)] and 2D [Fig. 3(b)], assuming high background doping. Whereas in the 3D case [Fig. 3(a)], the shape of the initial distribution is conserved, in 2D [Fig. 3(b)] the distribution broadens with time and exhibits anomalously fast diffusion behavior [3]. In this case the width of the distribution $L \propto t^{1/2}$. The effective diffusion coefficient D_{eff} is proportional to the carrier density which can be set equal to the background doping p_0 in the linear regime. If the injected perturbation becomes large compared to the doping
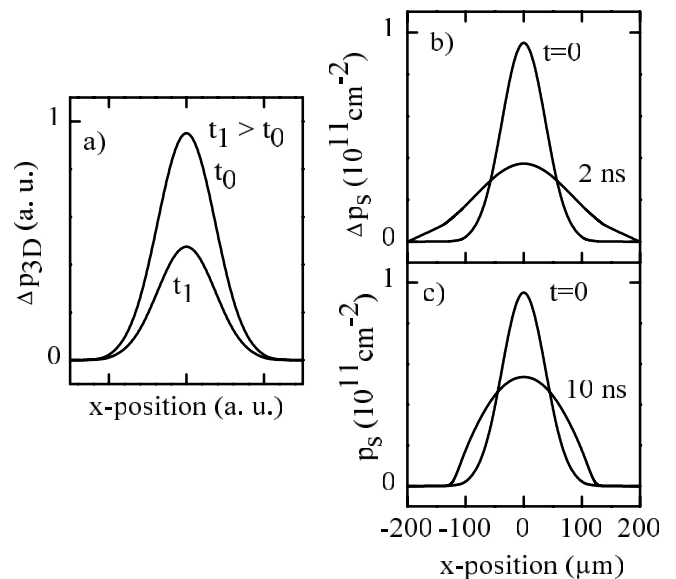

FIG. 3. Comparison of 3D relaxation in the linear regime (a) with the linear regime in 2D (b) and the nonlinear case discussed here. For (b), a constant doping of 6×10^{11} cm^{-2} is assumed. For (b) and (c), a constant mobility of 6×10^4 cm^2/V s has been used.
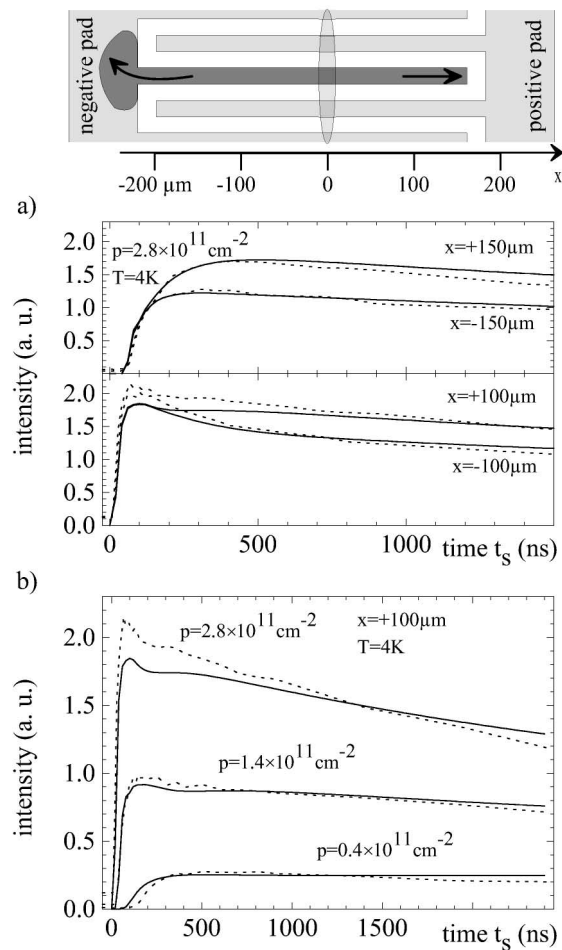
FIG. 4. Temporal evolution of the luminescence intensity at fixed locations on the sample, as indicated. In (a), for $x = \pm 100$ μm and $x = \pm 150$ μm, the influence of the different boundary conditions on either side of the laser spot is clearly visible. In (b), we show the dependence of the temporal evolution on the initial charge density. The dashed lines (experiment) and solid lines (theory) exhibit very good agreement.

concentration or in the case without doping, this is no longer true and the problem becomes nonlinear. As we can estimate $D_{eff} \sim \langle p \rangle \sim \frac{Q_0}{L}$ with the total amount of injected charge Q_0 and the spatially averaged distribution $\langle p \rangle$, D_{eff} decreases with time, retarding the dynamic process. The shape of the resulting carrier distribution is considerably compressed. Now, as the width of the distribution $L \propto \sqrt{\langle D_{eff} \rangle t}$, L is proportional to $t^{-1/3}$.

A comparison of the model to our experimental data (dashed lines) in this strongly nonlinear regime is given in Fig. 4. Now, the development of density with time at a fixed position is plotted. The simulation incorporates the initial laser pulse of 15 ns and the boundary conditions of the ideal sink and the hard wall at $x_{sink} = -200$ μm and $x_{wall} = +180$ μm, respectively. The experimental curves have been fitted using exclusively the mobility as a free parameter, which was assumed to be constant in the investigated density range. In all graphs, experimental and theoretical data correspond very well, indicating that the assumptions made are accurate. Especially, we were able to determine the mobility of holes in our undoped sample to about 60×10^3 cm(V s)$^{-1}$, being comparable to modulation doped structures [17]. We therefore deal with a very suitable model system for charge relaxation in two dimensions.

Figure 4(a) demonstrates the strong influence of the boundaries at a fixed initial density. A remarkable feature in the plot for $x = +100$ μm is the additional hump at $t_s \approx 400$ ns, which occurs as the moving hole distribution is reflected from the hard wall at the boundary. In Fig. 4(b), solutions for several densities at a fixed position near the hard wall are shown. Again, all curves exhibit very good quantitative agreement between theory and experiment. Here, the slowdown on a long time scale is very apparent. In addition, a considerable deceleration occurs with decreasing initial concentration, as, again, the repulsive forces decrease with density.

To sum up, we have presented experimental and theoretical investigations of the charge dynamics in an undoped QW structure with a lateral voltage-controlled superlattice. This system is an almost perfect model for unipolar 2D relaxation: Major features of the spreading character and the density dependence have been demonstrated. In addition, the influence of different boundary conditions could be studied.

[1] cf., e.g., S. M. Sze, *Physics of Semiconductors* (Wiley, New York, 1981), Chap. 7.
[2] M. I. D'yakonov and A. S. Furman, Sov. Phys. JETP **65**, 574 (1987).
[3] A. V. Chaplik and A. O. Govorov, Surf. Sci. **196**, 719 (1988); A. O. Govorov and A. V. Chaplik, Sov. Phys. JETP **68**, 1143 (1989).
[4] V. E. Arkhincheev, Sov. Phys. JETP **72**, 445 (1991).
[5] J. R. Haynes and W. Shockley, Phys. Rev. **81**, 835 (1951).
[6] K. H. Gulden et al., Phys. Rev. Lett. **66**, 373 (1991).
[7] M. Beck et al., Phys. Rev. B **64**, 085307 (2001).
[8] A. Schmeller et al., Appl. Phys. Lett. **64**, 330 (1994).
[9] H. Drexler et al., Appl. Phys. Lett. **64**, 2270 (1994).
[10] S. Zimmermann et al., Phys. Rev. B **56**, 13414 (1997).
[11] G. H. Döhler, Festkörperprobleme **XXIII**, 207 (1983).
[12] C. Rocke et al., Phys. Rev. Lett. **78**, 4099 (1997).
[13] S. Zimmermann et al., Science **283**, 1292 (1999).
[14] S. K. Zhang et al., Appl. Phys. Lett. **77**, 4380 (2000).
[15] The complete animated sequence of the images can be found at http://www2.nano.physik.uni-muenchen.de/~krauss/spread.html
[16] A. V. Chaplik, Sov. Phys. JETP **35**, 395 (1972); W. R. Frank et al., Phys. Rev. B **55**, R1950 (1997).
[17] T. S. Cheng et al., J. Vac. Sci. Technol. B **12**, 2621 (1994).